# DETECTION OF CECAL CONTAMINANTS IN VISCERAL CAVITY OF BROILER CARCASSES USING HYPERSPECTRAL IMAGING

B. Park, K. C. Lawrence, W. R. Windham, D. P. Smith

**ABSTRACT.** *Detecting fecal contaminants in the visceral cavity of the broiler is difficult but extremely important for poultry safety inspection. A hyperspectral imaging system was used for detecting internal cecal contaminants on broiler carcass halves. Two 565- and 517-nm wavelength images were selected from 512 calibrated hypercube image data. Image processing algorithms including band ratio, threshold, and median filtering were used to identify fecal contaminants from the internal cavity. The accuracy of detection algorithms to identify cecal contaminants varied with fecal threshold values and median filter as well. The imaging system identified cecal contaminants with 92.5% detection accuracy but also incorrectly identified 123 carcass features that were not considered as contaminants (false positives) and missed 15 actual contaminants when a fecal threshold value of 1.05 was employed. The higher accuracy (96.9%) and lower missed contaminants were obtained when a different fecal threshold value was used. However, in this case, false positives markedly increased.*

***Keywords.*** *Machine vision, Image processing, Food safety, Poultry inspection, Hyperspectral, Multispectral imaging, Fecal contamination, Ceca, Internal contaminants.*

Food safety, in particular the control of food borne pathogens, has become an important driving force for the federal government. Reduction in the potential health risks to consumers from human pathogens in food is the most important food safety issue and public concern. About 4000 deaths and 6.5 to 33 million illnesses in the United States each year are food related. The USDA estimates that medical costs and productivity losses resulting from pathogens in food range between $6.5 billion and $34.9 billion annually (FSI, 1997).

The Food Safety and Inspection Service (FSIS) pursue a broad and long-term science-based strategy to improve the safety of poultry and poultry products to better protect public health. In FY 1995, FSIS inspected more than 7 billion poultry. The task of inspecting meat and poultry is important because consumers spend $120 billion, or one-third of their annual food dollars, on meat and poultry products. Inspectors check animals before and after slaughter, preventing diseased animals from entering the supply and examining carcasses for visible defects that can affect safety and quality.

The rule on Pathogen Reduction and Hazard Analysis and Critical Control Point (PR/HACCP) Systems finalized by FSIS (USDA, 1996) targets pathogens that cause food-borne illness, strengthens industry responsibility to produce safe food, and focuses inspection and plant activities on prevention objectives.

The purpose of HACCP systems is to identify potential food safety hazards arising in slaughter and processing plants. HACCP is a system of steps used to identify and prevent problems from occurring during food processing and to correct them as soon as they are detected. With HACCP in place, FSIS can verify that the plant is controlling its processes and consistently producing products that comply with food safety requirements. Under HACCP, more than 8000 inspection operations employees, including more than 1100 veterinarians, carry out the inspection laws in over 6400 privately-owned meat, poultry, and other slaughtering or processing plants in the United States. Currently, the inspection system is based largely on organoleptic traits, especially what inspectors could see: diseases, defects, and contamination on poultry carcasses. This inspection process is prone to human errors due to fatigue, variability, and different appreciation, etc. The FSIS is changing the federal meat and poultry inspection system from a system based primarily on sight, touch, and smell to one incorporating scientific testing and systematic prevention of contamination.

The FSIS published a proposed rule, "Enhanced Poultry Inspection" (USDA, 1994) to clarify and strengthen the Agency's zero-tolerance policy for visible fecal contamination on poultry carcasses. Prior to this rule, FSIS ensured removal of all visible fecal contamination subsequent to postmortem inspection through off-line reinspection, direct on-line observations by an inspector, and application of finished product standards.

Without proper procedures during slaughter and processing, the edible portions of the carcass can become contaminated with bacteria capable of causing illness in humans. Preventing carcasses with visible fecal contamination from entering the chiller is critical for preventing cross-contamination of other carcasses. The final carcass wash before the

Article was submitted for review in January 2004; approved for publication by the Food & Process Engineering Institute Division of ASAE in February 2005. Presented at the 2003 ASAE Annual Meeting as Paper No. 033021.

Mention of any company or trade is for description only and does not imply endorsement by the U.S. Department of Agriculture.

The authors are **Bosoon Park, ASAE Member,** Research Agricultural Engineer, **Kurt C. Lawrence, ASAE Member,** Research Agricultural Engineer, **William R. Windham, ASAE Member,** Research Animal Physiologist, and **Douglas P. Smith,** Research Food Technologist, USDA, ARS, Richard B. Russell Research Center, Athens, Georgia. **Corresponding author:** Bosoon Park, USDA, ARS, Richard B. Russell Research Center, Athens, GA 30604-5677; phone: 706-546-3396; fax: 706-546-3633; e-mail: bpark@saa.ars.usda.gov.

carcasses enter the chiller is a critical control point for preventing cross-contamination of other carcasses.

With the HACCP system, industry was mandated to establish science-based process controls. The detection of fecal and ingesta contamination by visual observation is far from a science-based approach to process control. In addition, there has been a dramatic increase in water usage in most plants as a result of the zero tolerance standards. Plants have nearly doubled their previous water usage and nationwide, the usage has increased an estimated 2 billion gallons (Jones, 1999). Therefore, development of machine vision technology that retains individual carcass inspection for on-line detection of fecal and ingesta contamination would provide a science-based process control and decrease water usage.

Imaging spectroscopy or hyperspectral imaging, which is one of the most advanced machine vision technologies in reference to the multispectral character of the data set, refers to the imaging of a scene over a large number of discrete, contiguous spectral bands such that a complete reflectance spectrum can be obtained for the region being imaged. The reflectance spectra of food materials on the surface contain characteristic or diagnostic absorption features. Reflectance spectrum absorption features can be used to identify a number of important spectral characteristics of surface contaminants such as feces.

Since the late 1990s, hyperspectral imaging has emerged as a powerful technique in medical, biological, and remote sensing applications (Schowengerdt, 1997; Levenson et al., 1998; Burman, 1999; Dwyer and DiMarzio, 1999; Arnoldussen et al., 2000; Malkoff and Oliver, 2000; Inoue et al., 2001; Spillman et al., 2001; Zuzak et al., 2002).

In the agricultural side, hyperspectral imaging technologies were applied for grass characterization, sugar contents in melon, apple bruise detection, wheat scab detection, and poultry fecal detection (Heitschmidt et al., 1998; Schut et al., 2002; Tsuta et al., 2002; Lu et al., 1999; Delwiche and Kim, 2000; Kim et al., 2001; Mehl et al., 2001; Windham et al., 2002, 2003b; Lawrence et al., 2002, 2003; Park et al., 2003a, 2003b).

According to the previous study (Windham et al., 2003b), hyperspectral imaging has been proved as a useful tool to thoroughly analyze the spectra of inhomogeneous materials that contain a wide range of spectral and spatial information. Also, it was an effective technique for identifying surface contaminates on poultry carcasses. Previously, hyperspectral and multispectral imaging techniques have been applied to detect fecal contaminants on the surface of poultry carcasses (Lawrence et al., 2002; Park et al., 2003a, 2003b; Windham et al., 2003b). However, in order to successfully implement hyperspectral imaging techniques for poultry inspection, internal fecal contaminants, which might occur during processing, must be detected. Therefore, the purpose of this research is to examine a hyperspectral imaging system for detecting fecal contaminants in the visceral cavity of broiler carcasses.

## Materials and Methods

### Materials

The experiment was conducted on five separate days from October 2002 until April 2003 with 10 birds imaged each day for a total of 50 birds. Fifty 'New York Dressed' broiler carcasses were obtained from a local processing plant in Athens, bagged and transported to the Russell Research Center pilot-scale processing facility for evisceration and measurement. Prior to imaging, birds were hand eviscerated and manually washed both internally and externally. Digestive material from the cecal portions of the digestive tract from each carcass were collected and stored in plastic containers. Since cecal feces are dark brown, paste and the color is more consistent compared to other feces such as duodenum and colon, cecal feces were used for experiments as internal contaminants. For the convenience of imaging carcasses, all carcasses were cut in half to expose internal carcass to the camera. To minimize dehydration effect of surface, all carcasses were imaged from 1 to 3 h after slaughter.

### Hyperspectral Imaging System

A hyperspectral imaging system was designed and constructed to collect spectral images of poultry carcasses (Park et al., 2003b). A transportable imaging cart was designed to provide both portability and flexibility in positioning both the lights and the camera system (fig. 1). The cart was also designed to contain a computer, power supplies, and other equipment. Lighting requirements such as intensity and distribution were evaluated and adjusted for quality image acquisition. The imaging system consists of an imaging spectrograph with 25-μm slit width and an effective slit lengths of 8.8-mm − Grating Type I (ImSpector V9, PixelVision, Beaverton, Oreg.); a high resolution CCD camera (SensiCam Model 370KL, Cooke Corp., Auburn Hills, Mich.); 1.4/23-mm compact C-mount focusing lens, (Xenoplan, Schneider, Hauppauge, N.Y.) and associated optical hardware (Mao, 2000); motor for lens motion control (Model RSP-2T, Newport Corp., Irvine, Calif.); frame-grabber (12-bit PCI interface board, Cooke Corp., Auburn Hills, Mich.); and computer (Pentium II, 500 MHz). The prism-grating-prism spectrograph has a nominal spectral range of 430 to 900 nm with 6.6-mm axis and attaches to the camera for generating line-scan images. The spectrograph has a nominal spectral resolution of 2.5 nm. It is connected to a 2/3-in. silicon based CCD sensor with a 1280- × 1024-pixel resolution. The camera was thermoelectrically cooled and had a spectral response from 290 to 1000 nm with a maximum readout time of 8 fps. For consistent illumination of poultry carcasses, the lighting system consists of the 150-W quartz halogen DC stabilized fiber optic illuminator (Fiber-Lite A240, Dolan-Jenner, Inc., Lawrence, Mass.), lamp assembly, fiber optic cables, and 10-in. illuminating size of quartz halogen line lights (QF5048, Dolan-Jenner, Inc., Lawrence, Mass.).

### Spectral and Spatial Calibration

To fully characterize the spectral and spatial nature of the hyperspectral imaging system, a full calibration, considering both spectral and spatial information, is required. The hyperspectral imaging system was calibrated both spectrally and spatially as reported earlier (Lawrence et al., 2003). For spectral calibration of the hyperspectral imaging system, a 12-in. (0.31-m) integrating sphere (Model OL-455-12-1, Optronic Laboratories, Inc., Orlando, Fla.) was used as a spatially uniform target. Spectral calibration lamps and lasers

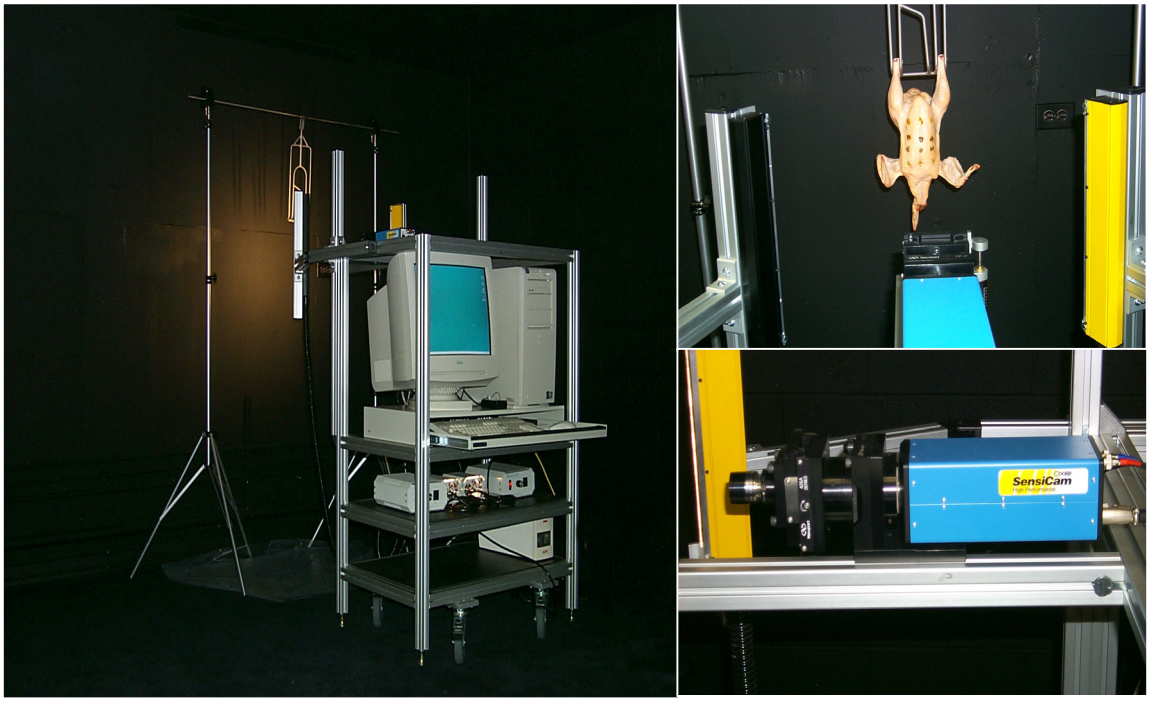


**Figure 1. Transportable hyperspectral imaging system.**

were used as spectral calibration standards. Mercury-Argon (Model 6035, Oriel Instruments, Stratford, Conn.) and Krypton (Model 6031, Oriel Instruments, Stratford, Conn.) calibration lamps were used with Oriel 6060 DC Power Supply to provide calibration wavelengths from about 400 to 900 nm. A Uniphase Helium-Neon Laser (Model 1653) and Melles Griot Helium-Neon Laser (Model 05-LHR-151) were also used as spectral standards at 543.5 and 632.8 nm, respectively.

For spatial calibration, thin vertical lines were made on a transparent film with a 1-mm center-to-center spacing. The vertical lines were positioned in front of the spectrograph with an Edmund XY stage and orifice.

Spectralon panels (Labsphere, Inc., North Sutton, N.H.) were used to calibrate and validate the hyperspectral imaging system to percent reflectance values. For calibration to percent reflectance values, a uniform 99% reflectance panel (SRT-99-100) and dark current measurements were used, and for validation, a gradient reflectance panel (SRT-MS-100) was used. The gradient panel consisted of evenly divided four vertical sections with nominal reflectance values of 99%, 50%, 25%, and 12%. Each panel was 10-in. square and effectively filled the entire viewing area of the imaging system with positioned about 50.8 cm (20 in.) from the focusing lens. System calibration resulted in wavelength errors of less than 0.5 nm and distance errors to less than 0.01 mm (relative to slit length). The pixel-by-pixel percent reflectance calibration, which was performed at all wavelengths with dark current and 99% reflectance calibration-panel measurements, resulted in errors generally less than 5% at the mid-wavelength measurements between 430 and 850 nm (Lawrence et al., 2003)

## PROCEDURES

Prior to image acquisition of each experiment, HyperVisual Software (ProVision Technologies, Stennis Space Center, Miss.) was used to focus the camera and align the fiber-optic line lights to provide uniform illumination across the calibration panels. For calibration and validation purpose, 99% reflectance panel, gradient panel, and dark current measurements were conducted in sequence at the beginning and the end of each experiment.

Broilers were eviscerated manually and cecal samples were collected as described earlier. To minimize oxidation and dehydration of the samples, broilers were stored in plastic bags prior to imaging. Each carcass was manually cut in halves for easy imaging of the visceral cavity of the broiler carcass. Carcass halves were hung on a standard evisceration shackle, which was welded to a stainless steel support rod to expose cavity to the camera for imaging. A laser pointer was used to align fiber optic line light propagation to make light diffuse on the carcasses as much as possible. Light intensity and distribution on the carcasses were measured and optimized using a digital intensity meter (Mavolux 5032C, Gossen, Germany) before image was collected. HyperVisual software was used to control the camera, which was set at 4 × 2 binning resulting in 320 horizontal spatial pixels and 512 vertical spectral pixels measured per line-scan image. The spectral resolution of hyperspectral images was approximately 0.9 nm and a total of file size of each image was 121 Mb. Even if scanning time depends on the size of a carcass, the average time to scan each sample was about 38 s. to collect a 380 line-scan image (vertical spatial) with 50-ms exposure time. Thus, each hypercube image had 3-D data structure with 320 × 380 (spatial) and 512 (spectral) resolutions. After a clean carcass was imaged, cecal contaminants were applied to four different areas including fat, meat, bone, shade of the inside carcass. The clean poultry carcass and the application of the contaminants on the birds were also videoed so that the exact location of the contaminant could be documented for future reference.

### Hyperspectral Image Processing

Hyperspectral images and spectral image files were further processed, analyzed, and displayed using Environment for Visualizing Images (ENVI) software (Research Systems Inc., Boulder, Colo.). Once the hypercubes were created, the image data were also calibrated to percent reflectance values as reported earlier (Lawrence et al., 2003). The data were also spectrally smoothed by boxcar averaging over a 20-nm bandwidth with a custom program written in IDL (Interactive Data Language, Research Systems Inc., Boulder, Colo.), which was compiled and run from within ENVI. Each hypercube was calibrated by the following sequence for further image processing and analysis, i.e., data conversion from integer to floating point, geo correction, percent reflectance calibration, and wavelength calibration. All image processing and analysis was performed by batch mode and the following steps were executed on each smoothed image. First, the background was removed from the carcass image by applying a background threshold mask. Next a ratio image was created by dividing a 565-nm image by a 517-nm image. The ratio of these two wavelengths had been determined earlier to be well suited for the detection of surface fecal contaminants (Park et al., 2003b). The background mask was then performed for this ratio image and a contaminant thresholding was performed for masked-ratioed image to separate the contaminants from the inside of carcass halves. Finally a 3 × 3 median filter was applied to remove speckled noise. The initial contaminant threshold value was selected based on the results of image data analysis from the region of interest (ROI) collected from thigh, breast, wing, duodenum, ceca, colon, and ingesta (Windham et al., 2002). The total number of pixels above a selected threshold value was then recorded and the contaminant threshold value was tuned by the number of pixels above the contaminant threshold. Once the background and contaminant thresholds were determined, they were applied for batch mode image analysis of all carcasses, both clean and contaminated. All processed images, mask, ratio, masked ratio, threshold, and filtered, were saved for further comparison between clean and contaminated carcass halves.

## Results and Discussion

### Spectral Characteristics of ROI Hyperspectral Images

Figure 2 shows typical sample of poultry carcass halves with fecal contaminants. It is not easy to identify cecal contaminants except on contaminated skin. Actual contaminant size was very small, only 158 pixels (0.43% of a half carcass). Figure 2b shows ROI of contaminated and clean spots. Among four contaminants, only ROI marked in red was distinctive, and three other contaminants were invisible due to the similar color of background and shades. Actually, however, the ROIs in red (A), green (B), blue (C), and yellow (D) were contaminated with ceca, whereas the ROIs in cyan (E), magenta (F), maroon (G), and sea green (H) were clean.

Figure 3 is the corresponding spectra for ROIs (fig. 2b) including cecal contaminants, skin, meat, and bones from the carcass half in figure 2. Typically, the cecal spectra gradually increased with wavelength between 420 and 730 nm. While the reflectance spectra from skin, meat, and bones increased up to about 520 nm. After this point the spectra decreased and

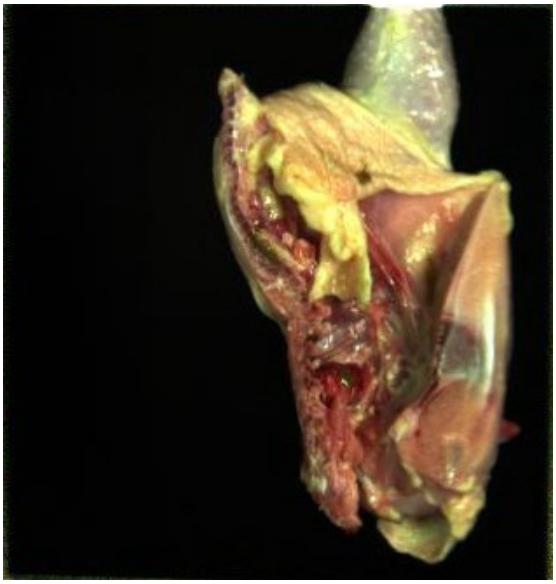

**(a)**

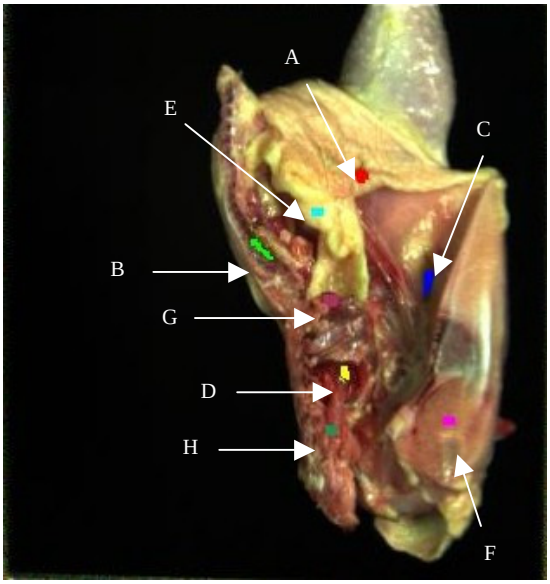


**(b)**

**Figure 2. ROI of chicken carcass halves (a) cavity with cecal contaminants; and (b) cavity with cecal contaminant ROI: red (40), green (39), blue (54), yellow (25); and clean ROI: cyan (30), magenta (30), maroon (46), and sea green (33). Note: numbers in the parenthesis represent pixel size of each labeled area. Total image size of carcass halves was 36,900 pixels.**

then increased again from the wavelength of about 550 nm. Especially, the reflectance spectra of skin were much higher than those of the contaminants and had peaks around 520 and 560 nm that were associated with the oxidative state of the myoglobin in the skin (Windham et al., 2003a). As shown in figure 3, the peaks of the spectra at 565 nm were always higher than peaks at 517 nm for contaminants, whereas non-contaminant spots had reverse trends. Therefore, the ratio of an image at 565 nm divided by an image at 517 nm would result in contaminants with values greater than one while non-contaminants would have values less than one.

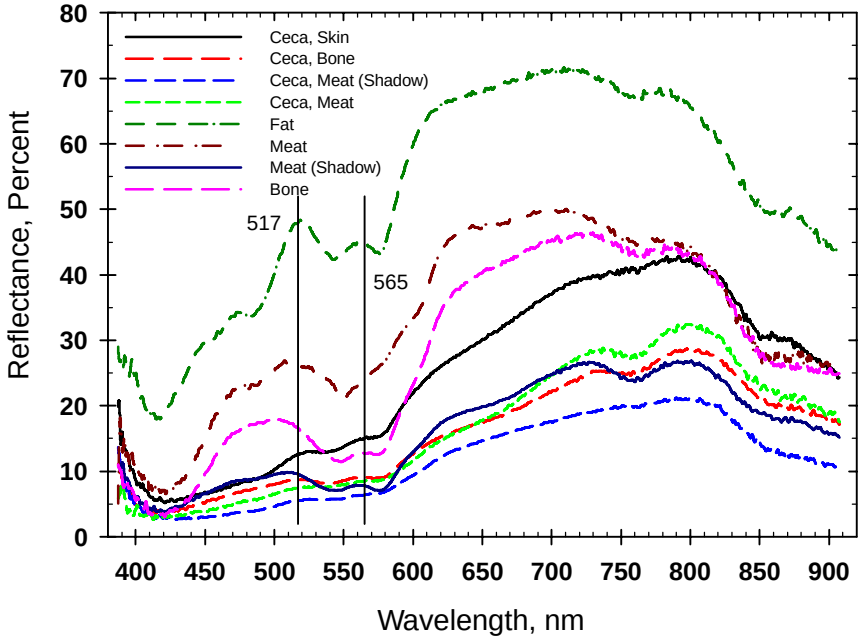


**Figure 3. Mean spectra of clean and cecal contaminant spots from inside of poultry carcass halves.**

Figure 4 shows reflectance mean spectra of the same ROI from skin, bone, and meat before and after cecal contaminants were applied. Typically, the reflectance spectra of non-contaminated area were higher than those of contaminated area except reflectance spectra from meat between 520 and 600 nm. Even if reflectance spectra of contaminants were lower than non-contaminants, the reflectance values at 565 nm were always higher than those values at 517 nm for contaminants. Thus, if the ratio of reflectance values at 565 nm divided by those values at 517 nm were greater than one, the pixel location is considered as a contaminant. As expected, the reflectance spectra of skin were much higher than those of bone and meat. Even if reflectance values of meat and bone were lower than those of skin, the reflectance values for non-contaminants of meat and bone ROI at 517 nm were higher than those at 565 nm.

### Selection of Threshold from ROI

To determine initial contaminant threshold value to classify contaminants, the results of ROI data analyses were used. ROIs of each carcass were selected at seven different locations including uncontaminated skins from the thigh, breast, and wing of the carcass, and duodenum, ceca, colon, and ingesta contaminants applied to the carcasses. From a total of 336 ROI data sets, the mean ROI reflectance spectra

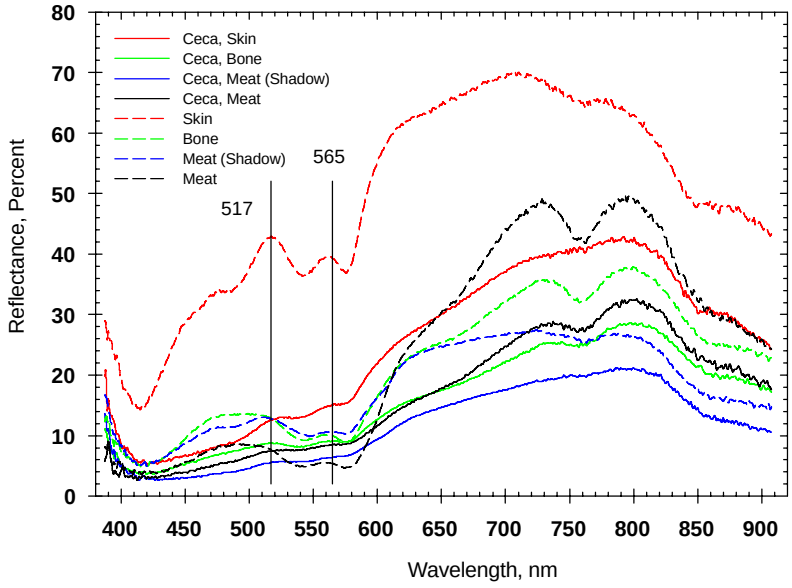


**Figure 4. Comparison of mean spectra before and after cecal contamination inside of poultry carcass halves.**

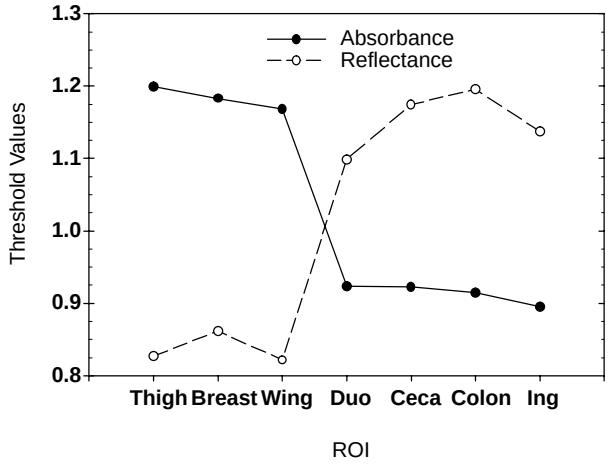


**Figure 5. Mean threshold values for differentiating contaminants (duodenum, ceca, colon, and ingesta) from clean poultry skin (thigh, breast, and wing) ROI.**

at each wavelength were calculated and transformed to log (1/reflectance) to obtain absorbance (Windham et al., 2002). Figure 5 shows mean threshold values to differentiate contaminants from uncontaminated skins using reflectance and absorbance of ROI spectra. For reflectance ROI, the threshold values to identify contaminants ranged from 1.09 to 1.19, which corresponded with absorbance of 0.89 and 0.92, respectively, whereas reflectance threshold values for uncontaminated skins ranged from 0.82 to 0.86, corresponding with 1.16 and 1.19 for absorbance. The initial threshold value for contaminant detection was determined based on the intersection of reflectance and absorbance. Thereafter, the threshold value of 1.0 was employed for ratioed images for further identifying contaminants in visceral cavity of broiler carcasses.

### Image Processing Algorithms

Figure 6 shows the results of image processing steps for fecal detection with a composite color image of a half carcass (fig. 6a) containing four cecal contaminants on skin, bone, meat, and shade in a cavity. Figure 6b is an image at 565 nm divided by an image at 517 nm and figure 6c is a mask to eliminate background noises created from a 633-nm image. Figure 6d is a ratioed image with the background mask applied. Figure 6e is the masked ratioed image with a fecal threshold of 1.025 and displays four distinctive contaminants as well as three false positive spots, on the leg (6 pixels), between skin and bone contaminants (4 pixels), and under the meat contaminant in the cavity (2 pixels), which could be eliminated by a 3 × 3 median filter (fig. 6f).

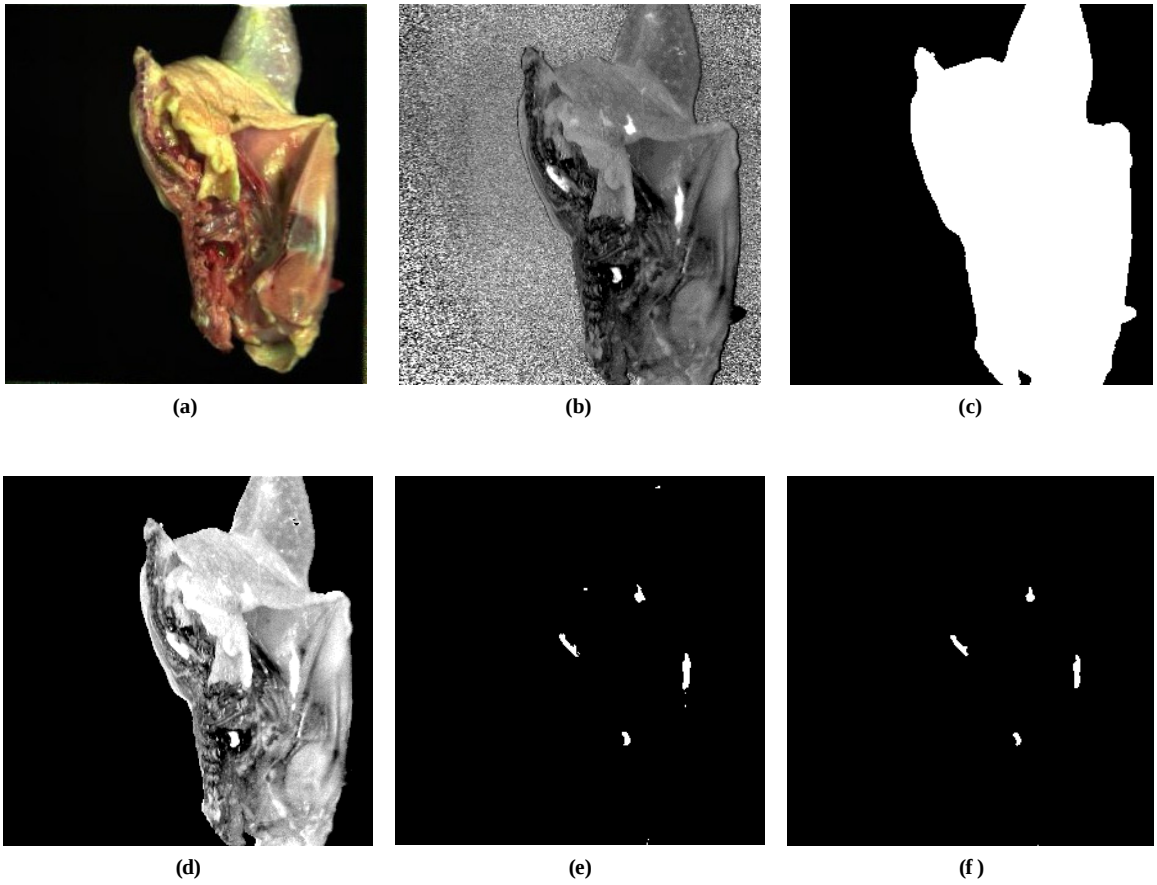


**Figure 6. Results of batch image processing with 4 × 2 binning, 125-ms exposure time, calibrated hyperspectral image of (a) color composite image of typical internal cecal contaminated carcass, (b) wavelength (565/517) ratio image, (c) background mask, (d) masked-ratio image, (e) fecal threshold (T =1.025) image, and (f) fecal threshold with median filter image.**

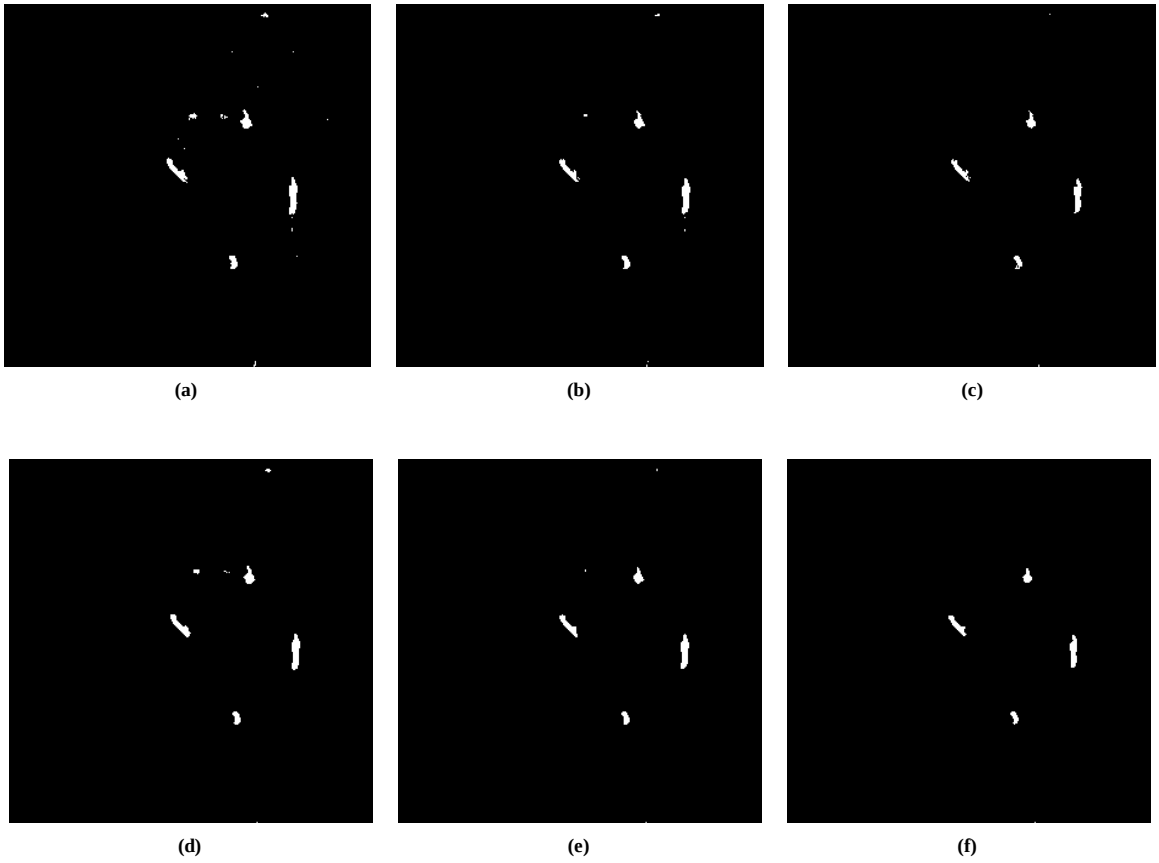


**Figure 7. Results of batch image processing of hyperspectral images for identifying internal fecal contaminants of broiler carcasses: (a) T = 1.0 with no filter; (b) T = 1.025 with no filter; (c) T = 1.05 with no filter; (d) T = 1.0 with median filter; (e) T = 1.025 with median filter; and (f) T = 1.05 with median filter.**

### Comparison of Cecal Contaminant Detection Thresholds

Figure 7 shows the results of batch image processing with three threshold values and median filter. Initially, we applied the threshold value of 1.0 chosen by the method described in the previous section for carcass halves images (n = 50) for cecal contaminant detection. Threshold value of 1.0 detected four contaminants distinctively, but contained 12 false positives (fig 7a). When a median filter was applied for this threshold image, still three false positives remained (fig 7d), which implied that 1.0 threshold value was not optimum in this case. Therefore, other threshold values were examined to determine the optimum threshold value for detecting cecal contaminants in visceral cavity of broiler carcasses. When the threshold value of 1.025 was used, all contaminants were detected correctly with four false positives (fig. 7b), and two false positives with median filter applied (fig. 7e). Figure 7c shows processed image with 1.05 threshold value. Four contaminants were detected with only one false positive in this case and finally same threshold value with median filter shows four contaminants only without false positive (fig. 7f).

### Accuracy of Image Processing Algorithms for Detecting Cecal Contaminants

From the previous section we learned the accuracy of detecting algorithms depended on the determination of optimum threshold value. Table 1 shows the accuracy of detection algorithms with three different threshold values and median filter applied to 50 carcass halves. The accuracy varied from 75.9% to 96.95%. Among the total 195 contaminants, 189 contaminants were detected correctly (96.9%) with 1.0 fecal threshold, which was the highest accuracy of the detection algorithm in this study. But the accuracy decreased to 89.2% with median filter applied to the same images. When 1.025 fecal thresholding value was applied, the detection accuracy was 95.4% with no filter and 86.7% with median filter. Both accuracies decreased to 92.5% with no filter and 75.9% with median filter when fecal threshold value of 1.05 was applied for all image samples. Thus, the fecal threshold value selected from ROI study (Windham et al., 2002) could be used as an initial fecal threshold value for cecal contaminant detection in the visceral cavity of broiler carcasses.

**Table 1. Accuracy of internal cecal detection with different threshold values and median filter (total 50 carcass halves).**

| | Predicted Contaminants | | | | | |
|---|---|---|---|---|---|---|
| | Threshold = 1.0 | | Threshold = 1.025 | | Threshold = 1.05 | |
| Actual Contaminants | No Filter | Median Filter | No Filter | Median Filter | No Filter | Median Filter |
| 195 | 189 | 174 | 186 | 169 | 180 | 148 |
| % Accuracy | **96.9** | 89.2 | **95.4** | 86.7 | **92.5** | 75.9 |

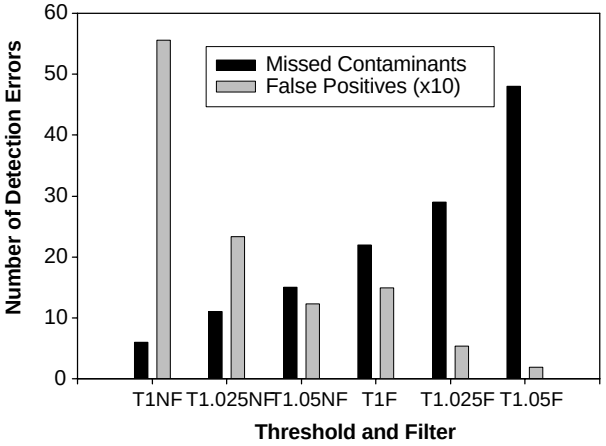


**Figure 8. Comparison of cecal detection errors with different fecal threshold values and median filter. Note: T1NF (threshold = 1.0, no filter), T1.025NF (threshold = 1.025, no filter), T1.05NF (threshold = 1.05, no filter), T1F (threshold = 1.0, median filter), T1.025F (threshold = 1.025, median filter), and T1.05F (threshold = 1.05, median filter).**

### Error Analysis for Cecal Detection

Figure 8 shows the comparison of cecal detection errors with different fecal threshold values and median filter. As fecal threshold values increased, the missed contaminants increased, whereas false positives drastically decreased. Fecal threshold with median filter derived more missed contaminants and less false positives when the results of the same fecal threshold images were compared. Fecal threshold value of 1.0 without median filter (96.9% accuracy, table 1) had the lowest missed contaminants (3.0% Type I error) and the highest false positives (556). However, in this case, more than half of false positives were counted from 1-pixel detection errors. When median filter was applied to the same images, the false positives drastically decreased to 149 but missed contaminants increased (11.2% Type I error). The fecal detection errors were sensitive to the fecal threshold values. When a fecal threshold value of 1.025 was applied to ratioed images, the missed contaminants increased (5.6% Type I error) even if false positives decreased to 233. The missed contaminants increased (14.8% Type I error) and false positives decreased to 53 when median filter was applied to the same threshold images. When fecal threshold value of 1.05 was applied to the images, the missed contaminants increased (7.6% Type I error) and false positive decreased to 123. With median filter applied to the same images, false positives decreased to only 19, which was the lowest in the experiments, whereas the missed contaminants drastically increased (24.6% Type I error), which was the highest. Thus, the accuracy of fecal threshold was trade off between missed contaminants and false positives. Therefore, optimum parameter values, especially fecal threshold values and filtering algorithms, need to be chosen for the purpose of the application. For this purpose, dynamic threshold methods need to be developed for determining the optimum threshold for different applications in poultry processing plants.

## Conclusions

A hyperspectral imaging system was validated for hypercube data acquisition of poultry carcass halves. The imaging system could identify internal fecal contaminants, especially cecal contaminants in the visceral cavity of broiler carcasses. Accuracy of the algorithm to identify contaminants varied with fecal threshold values and median filter. Among the three selected threshold values, as fecal threshold values increased, the missed contaminants increased whereas false positives decreased. The same trends occurred when median filter was applied to the same fecal threshold images. The imaging system identified cecal contaminants with 92.5% but also incorrectly identified 123 carcass features that were not considered as contaminants (false positives) and missed 15 actual contaminants (7.6% Type I error). Since only ceca was used for the experiments, additional studies should be conducted with different type of feces from digestive tracts such as duodenum and colon to validate image processing algorithms for detecting different sources of fecal contaminants in the visceral cavity of broiler carcasses. This study only used halved carcasses for image acquisition; however, whole birds must be inspected in the poultry processing line. Therefore, mechanical vent opener or equivalent devices to expose the cavity of carcasses to the camera as much as possible would help to detect internal contaminants during on-line processing.

## References

Arnoldussen, M. E., D. Cohen, G. H. Bearman, and W. S. Grundfest. 2000. Consequences of scattering for spectral imaging of turbid biologic tissue. *J. Bimed. Opt.* 5(3): 300-306.

Burman, J. A. 1999. Hybrid pattern recognition method using evolutionary computing techniques applied to the exploitation of hyperspectral imagery and medical spectral data. *Proc. SPIE* 3871: 348-357.

Delwiche, S. R., and M. S. Kim. 2000. Hyperspectral imaging for detection of scab in wheat. *Proc. SPIE* 4203: 13-20.

Dwyer, P. J., and C. A. DiMarzio. 1999. Hyperspectral imaging for dermal hemoglobin spectroscopy. *Proc. SPIE* 3752: 72-82.

FSI. 1997. The Food Safety Initiative's Report to the President. May 1997.

Heitschmidt, J., M. Lanoue, C. Mao, and G. May. 1998. Hyperspectral analysis of fecal contamination: A case study of poultry. *Proc. SPIE* 3544: 134-137.

Inoue, Y., J. Penuelus, Y. Nouevllon, and M. S. Moran. 2001. Hyperspectral reflectance measurements for estimating eco-physiological status of plants. *Proc. SPIE* 4151: 153-161.

Jones, F. T. 1999. Zero tolerance for fecal spots: FSIS. *Poultry* 6: 38-41.

Kim, M. S., Y. R. Chen, and P. M. Mehl. 2001. Hyperspectral reflectance and fluorescence imaging system for food quality and safety. *Transactions of the ASAE* 44(3): 721-729.

Lawrence, K. C., W. R. Windham, B. Park, and D. P. Smith. 2002. Contaminant detection on poultry carcass surfaces. *New Food* 5(3): 21-24.

Lawrence, K. C., B. Park, W. R. Windham, and C. Mao. 2003. Calibration of a pushbroom hyperspectral imaging system for agricultural inspection. *Transactions of the ASAE* 46(2): 513-521.

Levenson, R. M., E. S. Wachman, W. Niu, and D. L. Farkas. 1998. Spectral imaging in biomedicine: A selective overview. *Proc. SPIE* 3438: 300-312.

Lu, R., Y. R. Chen, B. Park, and K. H. Choi. 1999. Hyperspectral imaging for detecting bruises in apples. ASAE Paper No. 993120. St. Joseph, Mich.: ASAE.
Malkoff, D. B., and W. R. Oliver. 2000. Hyperspectral imaging applied to forensic medicine. *Proc. SPIE* 3920: 118-128.
Mao, C. 2000. Focal plane scanner with reciprocating spatial window. U.S. Patent No. 6,166,373.
Mehl, P. M., K. Chao, M. S. Kim, and Y. R. Chen. 2001. Detection of contamination on selected apple cultivars using reflectance hyperspectral and multispectral analysis. *Proc. SPIE* 4206: 201-213.
Park, B., K. C. Lawrence, W. R. Windham, and D. P. Smith. 2003a. Assessment of hyperspectral imaging system for poultry safety inspection. *Proc. SPIE* 4879: 269-279.
Park, B., K. C. Lawrence, W. R. Windham, and R. J. Buhr. 2003b. Hyperspectral imaging for detecting fecal and ingesta contaminants on poultry carcasses. *Transactions of ASAE* 45(6): 2017–2026.
Schowengerdt, R. A. 1997. Remote sensing: models and methods for image processing. San Diego: Academic Press.
Schut, A. G. T., J. J. M. H. Ketelaars, and J. Meuleman, 2002. Novel imaging spectroscopy for grass sward characterization. *Biosystems Engineering* 82(2): 131-141.
Spillman, W. B., Jr., K. E. Meissner, S. C. Smith, S. Conner, and R. O. Claus. 2001. Cellular automata for the analysis of biomedical hyperspectral images. *Proc. SPIE* 4259: 29-35.
Tsuta, M., J. Sugiyama, and Y. Sagara. 2002. Near-infrared imaging spectroscopy based on sugar absorption for melons. *J. Agri. Food Chem.* 50(1): 48-52.
USDA. 1994. Enhanced poultry inspection. Proposed Rule. *Fed. Reg.* 59: 35659.
USDA. 1996. Pathogen reduction; hazard analysis and critical control point (HACCP) systems. Final Rule. *Fed. Reg.* 61: 28805-38855.
Windham, W. R., K. C. Lawrence, B. Park, D. P. Smith, G. H. Poole. 2002. Comparison of spectra collected with a spectrophotometer and a hyperspectral imaging system to detect poultry fecal and ingesta contamination. ASAE Paper No. 023136. St. Joseph, Mich.: ASAE.
Windham, W. R., K. C. Lawrence, B. Park, and R. J. Buhr. 2003a. Visible/NIR spectroscopy for characterizing fecal contamination of chicken carcasses. *Transactions of the ASAE* 46(3): 747-751.
Windham, W. R., K. C. Lawrence, B. Park, L. A. Martinez, M. A. Lanoue, D. A. Smith, J. Heitschmidt, and G. H. Poole. 2003b. Method and system for contaminant detection during food processing. U.S. Patent No. 6587575.
Zuzak, K. J., M. D. Schaeberle, and E. N. Lewis. 2002. Visible reflectance hyperspectral imaging: characterization of a noninvasive in vivo system for determining tissue perfusion. *Anal. Chem.* 74(9): 2021-2028.